Research Square

Preprints are preliminary reports that have not undergone peer review.
They should not be considered conclusive, used to inform clinical practice,
or referenced by the media as validated information.

A Pragmatic Pharmacophore Informatics Strategy to Discover New Potent Inhibitors Against Pim-3

Sudhir Reddy Peddi
Osmania University University College of Science
Ramalingam Kundenapally
Osmania University University College of Science
Sree Kanth Sivan
Osmania University Nizam College
Gururaj Somadi
Osmania University Nizam College
vijjulatha manga (vijjulathamanga@gmail.com)
Osmania University https://orcid.org/0000-0001-9056-8385

Research Article

Keywords: Pim-3,pharmacophore, virtual screening, homology modelling, molecular docking, binding free energy, indole derivatives, molecular dynamics.

Posted Date: December 6th, 2021

DOI: https://doi.org/10.21203/rs.3.rs-1112972/v1

License: This work is licensed under a Creative Commons Attribution 4.0 International License.
Read Full License

Abstract

Pim-3 (proviral integration site moloney murine leukemia virus-3) is an oncogene which encodes proteins belonging to serine/threonine kinase family, and PIM subfamily. It is generally over expressed in epithelial and hematological tumors. It is known to involve in numerous cellular functions such as cell growth, differentiation, survival, tumorigenesis and apoptosis. It also plays a crucial role in regulation of signal transduction cascades. Therefore it emerged as a hopefultherapeutic target for cancer treatment. In current study, indole derivatives having potent inhibitory activity against Pim 3 were taken and pharmacophore based virtual screening was carried out. A five point pharmacophore hypothesis with one hydrogen bond acceptor, one hydrogen bond donor and three aromatic rings i.e., ADRRR was developed with acceptable $R^2$and Q^2 values of 0.913 and 0.748 respectively. It was employed as a query and screening was conducted against Asinex and Otava lead library databases to screen out potent drug like candidates. The obtained compounds were subjected to SP, XP docking using 3D model of pim-3 which was constructed through comparative homology modelling and finally binding free energies were calculated for top hits. The docking and binding free energy studies revealed that six hit molecules showed higher binding energy in comparison to the best active molecule. Finally, MD simulations of the top hit with highest binding energy was carried out which indicated that the obtained hit N1 formed a stable complex with pim-3. We believe that these combined protocols will be helpful and cooperative to discover and design more potent pim-3 inhibitors in near future.

Introduction

Pim-3 a serine/threonine kinase which belongs to Ca^{+2} /Calmodulin-dependent protein kinase group is a member of provirus integrating site moloney murine leukemia virus (Pim) family. Initially pim-3 was recognised as a novel gene that is induced by depolarization (KID)-1 or forskolin in PC12 cells (a rat pheochromocytoma cell line)[1]. Later it was renamed as pim-3 owing to its high similarity with that of Pim family of kinases. In human genome pim-3 gene is located on chromosome 22q13 encoding a protein with 326 amino acids. Its molecular weight is approximately 35 kD [2, 3]. Pim-3 is mainly unregulated in endoderm derived tumor tissues and it is known to inhibit apoptosis and increase cell proliferation in solid and some haematological cancers [4–6]. Pim-3 phosphorylates the Ser-112 site of BAD [5, 6] in particular thereby inhibits apoptosis and promotes cancer progression. Additionally by increasing the phosphorylation of STAT3 [7] pim-3 promotes migration and invasion of melanoma cells. Moreover, pim-3 was known to be upregulated in Hepatocellular carcinoma (HCC) tumor tissues and the knockdown of pim-3 in hepatoma cells enhances apoptosis and attenuates cell proliferation [3].

Previous studies have shown that pim kinases including pim-3 are aberrantly expressed in several types of malignancies and helps in inducing tumorigenicity [3, 5, 6, 8, 9]. Over expression of pim-3 mRNA was found in nasopharyngeal carcinoma cell lines and in a group of human ewing family tumor cell lines.In addition, over expression of pim was also found in the premalignant and malignant lesions in the stomach, colon and liver compared with the normal tissues [3, 5, 6, 9]. Further, Pim-3 promotes EWS/FLI mediated NIH 3T3 tumorigenesis and hepatocellular carcinoma evident from mice studies [3, 10].

According to recent studies it also aberrantly expressed in PDAC cells. Pim-3 serves as positive regulator of STAT3 signalling in pancreatic cancer cells [11, 12] and is reported to be regulated by transcription factors such as ETS-1.

Computer aided drug discovery (CADD) techniques [13, 14] have paved a new way in the modern era for developing and designing new drugs. CADD methodologies proved to be cost effective and time saving in drug discovery processes [15]. Molecular modelling studies such as virtual screening, 3D QSAR, Pharmacophore modelling emerged as promising methods in exploring new leads with drug like properties. Pharmacophore modelling has been successfully employed in discovering new ALK, JAK2 and D2 inhibitors which are useful in the treatment of cancers such as non-small cell lung cancer (NSCLC) [16], cardiovascular and myeloproliferation disorders [17] and Parkinson's disease, Huntington's chorea, schizophrenia and tardive dyskinesia [18] respectively. Virtual screening technique gained popularity among scientific community as it decreased the number of hits to be experimentally studied. Furthermore pharmacophore based virtual screening abetted the development of specific inhibitors against EGFR and HER2 [19, 20]. Therefore in the present work we experimented pharmacophore based virtual screening followed by structure base virtual screening protocols to discover new potent inhibitors against pim-3.

Materials And Methods

Dataset

A dataset consisting of 57 indole derivatives reported as pim-3 inhibitors were taken for the present study to develop a 3D pharmacophore. The activity of these molecules ranged from 5.295 to 8.187and shared common experimental method [21–23]. The structures of these compounds were sketched in Maestro build panel and subsequently prepared using LigPrep module [24, 25]. OPLS-2005 force field was used to generate different conformers and low energy conformer of each ligand was taken for further study. The invitro inhibitory activity of these compounds reported in the literature were converted to pIC_{50} using the equation 1.

$pIC_{50} = -\log_{10}[IC_{50}]$ (1)

Pharmacophore Generation

PHASE (Pharmacophore alignment and scoring engine) in Schrodinger [26] was used for pharmacophore generation which actually uses scoring techniques and fine-grained conformational sampling to find a common pharmacophore hypothesis (CPH) [27]. The prepared compounds along with the pIC_{50} values were imported and divided into actives and inactives quondam to generate pharmacophore. The ligands with pIC_{50} greater than 7.730 were treated as actives and pIC_{50} lower than 6.325 as inactive and remaining as the intermediates with moderate biological activity. To determine common pharmacophore hypothesis, PHASE from active ligands employs a tree based partitioning technique [28]. PHASE is

equipped with a built in set of six pharmacophoric features (aromatic ring (R), positively ionisable (P), negatively ionisable (N), hydrophobic group (H), hydrogen bond acceptor (A) and hydrogen bond donor (D) [27] based on which pharmacophore hypotheses were developed and further utilized for 3D QSAR generation.

3d Qsar Model Generation

3D QSAR model was achieved through PHASE module of Schrodinger. A chemo metric technique named partial least square analysis (PLS) was used for achieving 3D QSAR model which quantifies the relation between the structure of molecules and experimental biological activities [29]. For generating a 3D QSAR model initially the dataset was divided into training and test set randomly, the training set was used for deriving 3D QSAR model as it portrayed structural features and biological activities. The test set molecules were used for validating the QSAR model [30]. The pharmacophoric features of the training set compounds were placed into a typical grid of cube of 1Å spacing [27], each cubes assigned with 0 (or) 1 bit to account for distinct pharmacophore features in the training set. Hence a single cube will be engrossed with more than one pharmacophoric site expanding one or more volume bits. Thus depending upon the occupation of various sites in the cube a single molecule will be expressed with a string of binary values. The biological activity values will be treated as dependent variables whereas binary values will be considered as independent variables for developing a 3D QSAR model employing PLS regression [27]. Therefore, a series of regression models will be generated by the PHASE [31]. The obtained 3D QSAR model was then verified using test set of molecules using various statistical parameters such as regression coefficient (R^2), cross-validated correlation coefficient (Q^2), variance ratio (F), standard deviation (SD), Pearson-R and RMSE (root mean square error) [27, 31].

Screening Of 3d Databases Using Pharmacophore Model

The developed PHASE model was used as a query and screening was conducted against Asinex and Otava lead library databases to screen out the novel lead molecules that match with the top pharmacophore hypothesis and gauge the predicted biological activities using the generated 3D QSAR model.

Homology Modelling And Dock Based Virtual Screening

The crystal structure of pim-3 is not available till date in the protein data bank hence the protein was modelled using the sequence information derived from Uniprot database [32] (Accession code: Q86V86). BLAST (Basic Local Alignment Search Tool) [33] was employed for finding the best template from protein data bank (PDB). Based on E value, Sequence identity and secondary structure similarities a template was selected and pair wise alignment was done with Clustal-X [34] in order to find out the similarities, identities, conserved regions and the differences between the target and the template. The human pim-1

(PDB id: 1XWS) showed a sequence similarity of 96% with pim-3. Modeller 9.13 [35] was used for generating a new three-dimensional structure and various homology models were built out of which the least energy model was taken for further studies. The generated model was analysed and validated with PROCHECK [36], Verify 3D [37] and ProSA [38]. The modelled protein is equivalent to the low resolution X-ray crystal structure since the sequence similarity between the template and target was greater than 80% [39].

GLIDE module [40] of the Schrödinger package was employed for carrying out the docking studies. It is regularly used for molecular docking studies which is a grid based ligand docking approach with notable amount of success. It can predict the protein-ligand binding modes with decent accuracy and has significantly contributed in identifying numerous potent drug like candidates against various targets [41, 42]. Initially a grid was created centring on the ligand within a cubic box using receptor grid generation panel available in the GLIDE. The default VanderWaals scaling was set to 0.9 [43] for non-polar atoms with a partial charge cut-off of 0.25. Later the molecules which were screened from Asinex and Otava lead library databases were subjected to docking using standard precision protocol. The top 20% of the ligands which showed high dock scores were taken and passed for extra precision (XP) docking. Finally, binding energies were computed for the top 2% of the ligands retrieved from XP docking.

Binding Free Energy Calculations

Molecular docking is not always fruitful (or) ultimate method for lead identification. Further, the ranking of molecules based on vigorous binding energy calculations proved to be more propitious than sheer XP dock score [44]. Therefore, molecular mechanics-generalized born surface area (MM/GBSA) calculations were carried out on the top hits obtained from XP docking using prime module available in the Schrodinger. The equation for calculating binding free energy is given below:

$\Delta G_{bind} = G_{complex} - [G_{ligand(unbond)} + G_{receptor(unbond)}]$

$= \Delta E_{MM} + \Delta G_{solv} + \Delta G_{SA}$

ΔE_{MM}= Difference in the energy between the protein ligand complex and sum of energies of the protein with ligand and without ligand.

ΔG_{solv}= Difference in the GBSA solvation energy between the protein ligand complex and sum of the solvation energies for the ligand and unliganded protein.

ΔG_{SA}= Difference in the surface energy between the protein ligand complex and sum of the surface energies for the ligand and uncomplexed protein.

Md Simulations

MD simulations were performed on the hit obtained from screening process (N1) using Desmond 3.8 [45]. The stability of docked complex and the effect of conformational changes on the binding interactions were studied. SPC (simple point change) water molecules [46] were used for soaking the complex in orthorhombic box of 15Å×15Å×15Å dimensions. The net charges of the system were balanced by adding oppositely charged ions and the salt concentration was kept 0.15 mol L^{-1} during the simulation process. The OPLS 2005 force field [47]was used where the system was minimized two times, initially with restraints on solute and later without any restraints. The limited memory Broyden-Fletcher-Goldfarb-Shanno (LBFGS) algorithm and steepest descent integrator were employed during minimization until the value concentredto 5 kcal $mol^{-1}Å^{-1}$. A small relaxation protocol of 12 and 24ps was applied on the system before proceeding to the extensive MD Simulations. The temperature and pressure were maintained at 310K and 1.01325 bars respectively using Nose-Hoover thermostat and Martyana-Tobaisklein approach. The long range electrostatic interactions were computed using particle-mesh Ewald method [48] and cut off distance was curtailed to 9Å for calculating non-bonded interactions. The SHAKE algorithm [49] was exercised on all bonds enmeshed with H-bonds. Finally 10 ns MD simulations at NPT conditions were carried out and unblemished classical trajectories were recorded. The simulation interaction diagrams and root mean square deviation (RMSD) plots were generated from the trajectories in order to inspect the consistency and stability of various protein-ligand interactions.

Results And Discussion

Description of the generated Pharmacophore

The Pharmacophore model was generated using a set of ten active (pIC_{50} > 7.730) ligands in the dataset with the help of PHASE module available in Schrodinger suite. These active set of ligands may contain structural features which are essential for binding to the active site of pim-3 [50]. The structural and biological activity of pim-3 inhibitors taken for our analysis is depicted in Table 1. The variant list was determined by assigning maximum and minimum number of site to 5 after creating pharmacophore sites for all pim-3 inhibitors. The pharmacophore hypotheses (CPH's) identified in this process were scored and ranked according to the survival active and inactive scores by a scoring method in PHASE module. The inactive ligands though not used in CPH production they are used to eliminate the hypothesis that cannot extricate between actives and inactives [50]. Hence to achieve this purpose the obtained CPH's will be mapped onto the inactive ligands and scored. The hypothesis with good difference in survival active and survival inactive scores ADRRR was taken for further analysis as it clearly discriminates between active and inactive ligands. Among the generated models ADRRR was identified as the best hypothesis by scoring algorithm. The CPH with one H-bond acceptor (A2), one H-bond donor (D3) and three aromatic ring features (R9, R10 and R11) is shown in Figure 1. The distances and angles between various sites of the model are depicted in Figures 2 and 3, and tabulated in Supplementary Tables Tab S1 and Tab S2, respectively. Further, a 3D QSAR model was derived by pharmacophore based alignment of the ligands.

Table 1 Structures and biological activities of pim-3 inhibitors along with fitness scores based on pharmacophore hypothesis ADRRR

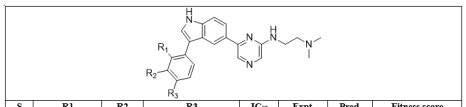

S No	R1	R2	R3	IC_{50} (μM)	Expt. pIC_{50}	Pred. pIC_{50}	Fitness score
1	H	H	CH_3	0.033	7.481	6.82	2.87
*2	H	CH_3	H	0.029	7.538	7.30	2.94
*3	H	H	CF_3	0.247	6.607	6.65	2.91
4	H	CF_3	H	0.069	7.161	7.24	2.86
5	H	H	NH_2	0.029	7.538	7.75	2.97
6	H	NH_2	H	0.040	7.398	7.54	2.94
7	H	H	CN	0.155	6.810	7.42	2.07
*8	H	CN	H	0.060	7.222	7.55	2.63
9	H	H	OCH_3	0.030	7.523	7.52	2.07
*10	H	OCH_3	H	0.019	7.721	7.26	2.26
11	H	OCF_3	H	0.128	6.893	7.15	2.22
*12	H	H	F	0.082	7.086	7.28	2.97
*13	H	F	H	0.035	7.456	7.54	2.65
14	F	H	H	0.010	8.000	7.68	2.65
15	H	H	C_6H_5	0.417	6.380	6.56	2.59
*16	H	H	SO_2CH_3	0.050	7.301	7.53	2.27
17	H	H	SO_2NH_2	0.026	7.585	8.01	2.27

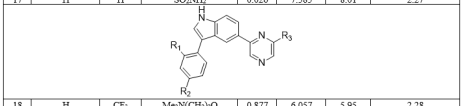

18	H	CF_3	$Me_2N(CH_2)_2O$	0.877	6.057	5.95	2.28
*19	H	CF_3	$Me_2N(CH_2)_2O$	0.905	6.043	6.00	2.76
*20	H	CF_3		0.204	6.690	6.43	1.46
21	H	CF_3	$Me_2N(CH_2)_3NH$	0.368	6.434	6.22	2.27
22	H	CF_3	$Me_2N(CH_2)_3NCH_3$	0.475	6.323	6.09	2.04
23	H	CF_3	$Me_2N(CH_2)_2NCH_3$	0.401	6.397	6.37	2.26
24	F	H	$HOCH_2CH_2$	3.050	5.516	5.87	2.83
25	F	H		0.016	7.796	7.64	2.28
26	F	H	$H_2N(CH_2)_3NH$	0.007	8.155	7.92	2.32

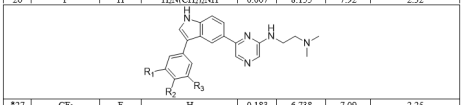

*27	CF_3	F	H	0.183	6.738	7.09	2.25
28	F	CF_3	H	0.589	6.230	6.63	2.9
*29	CN	NH_2	H	0.010	8.000	7.70	2.93

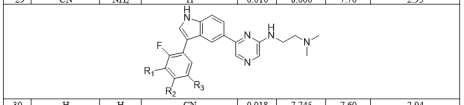

30	H	H	CN	0.018	7.745	7.60	2.94
31	H	H	$COCH_3$	0.007	8.155	8.11	2.58
*32	F	H	H	0.022	7.658	7.40	2.97
33	H	NH_2	H	0.009	8.046	7.78	3

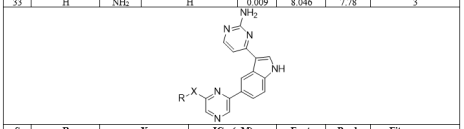

S No	R	X	IC_{50} (nM)	Expt. pIC_{50}	Pred. pIC50	Fitness score
34	Et	O	50.9	7.293	7.14	2.11
*35	$Me_2N(CH_2)_2$	O	21.7	7.664	7.32	2.04
36	$Et_2N(CH_2)_2$	O	30	7.523	7.57	1.66
37	$Me_2N(CH_2)_3$	O	20.5	7.688	7.66	1.82
*38	$Et_2N(CH_2)_3$	O	55.7	7.254	7.60	1.65
39	$Me_2N(CH_2)_2$	NH	6.5	8.187	8.23	1.91
40	$Et_2N(CH_2)_2$	NH	9.9	8.004	8.26	1.86
41	$Me_2N(CH_2)_2$	NH	31.3	7.504	7.61	1.67
*42	$Et_2N(CH_2)_2$	NH	30.2	7.520	8.10	1.86
43	$Me_2N(CH_2)_2$	NCH_3	7.8	8.108	7.87	1.66

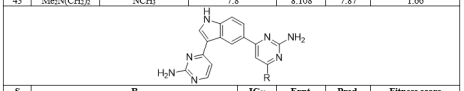

S No	R	IC_{50} (nM)	Expt. pIC_{50}	Pred. pIC50	Fitness score
44	$Me_2N(CH_2)_3O$	0.50	6.301	6.28	2.06
45	$Et_2N(CH_2)_3O$	0.27	6.569	6.45	2.62
*46	$Me_2N(CH_2)_3O$	0.16	6.796	6.42	2.05
47	$Et_2N(CH_2)_2O$	0.081	7.092	6.98	2.61
*48	$Me_2N(CH_2)_2NH$	0.47	6.328	6.45	1.76
49	$Et_2N(CH_2)_2NH$	0.33	6.481	6.50	1.69
50	$Me_2N(CH_2)_3NH$	0.24	6.620	6.44	1.70
51	$Et_2N(CH_2)_3NH$	0.61	6.215	6.34	1.68
*52		0.39	6.409	6.34	2.19
*53		0.74	6.131	6.11	2.63
54		0.37	6.432	6.39	2.44
55		1.26	5.900	5.83	2.64
56		5.07	5.295	5.72	2.63
57	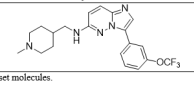	0.069	7.161	6.86	1.16

* Test set molecules.

Analysis Of 3d Qsar Model

The PHASE module of Schrodinger Suite was used to derive a pharmacophore based 3D QSAR model using the best CPH i.e. ADRRR. The derived 3D QSAR model will help in identifying all the features that are crucial for an inhibitor for its gross inhibitory activity against target pim-3 [50]. The dataset was randomly divided into 38 training and 19 test set (2:1) prior to the model generation. Subsequently with a grid spacing of 1Å the QSAR model was developed using PLS analysis. The t-set or eliminate variable was fixed to <2.0 during PLS regression analysis in order to eliminate those variables whose regression coefficients are very sensitive to tiny changes in the training set [51]. Three PLS factors in total were taken as further increase in the number did not improve the model statistics but over fitted [52]. The dominant statistics was observed with third PLS factor therefore it was chosen to create the QSAR model. To ensure the robustness of the developed model it was validated both internally and externally against training and test sets using R^2 and Q^2respectively [53, 54]. The $R^2$and Q^2 were found to be 0.913 and 0.748. The R^2 and Q^2 values greater than 0.6 and 0.5 indicates the model is sound and has high ability to predict inhibitory activities in training and test set [53, 55]. The model exhibited good statistical significance with Pearson R value of 0.880, variance ratio; F value of 101.2, low standard deviation; SD of 0.263and root mean square error; RMSE value of 0.286 [54]. The results are tabulated in Table 2. The experimental and predicted values of the entire dataset ligands are shown in Table 1. The 3D QSAR model was taken further for *insilico* screening in order to identify novel compounds with good inhibitory activity against pim-3.

Table 2
The statistical parameters of various pharmacophore hypotheses obtained through PHASE

ID	SD	R-squared	F	RMSE	Q-squared	Pearson-R
ADDPR	0.361	0.810	48.4	0.397	0.512	0.731
DDPRR	0.395	0.772	38.4	0.427	0.436	0.663
ADRRR	**0.263**	**0.913**	**101.2**	**0.286**	**0.748**	**0.880**
AADRR	0.401	0.766	37.1	0.440	0.401	0.667

3d Qsar Visualization Of Best Active Compound

The relationship between structure and activity relationship (SAR) and biological activity can be best understood with the help of three dimensional envision of best hypothesis ADRRR and selected indoleligands in aspect of developed QSAR. The 3D QSAR envision of best active compound (compound 39) with biological activity of 6.5 nM (pIC_{50} = 8.187) is shown Figure 4. In Figure 4a, b andc, blue and pink cubes represent hydrogen bond acceptor favoured and disfavoured regions respectively, yellow and orange cubes represent hydrogen bond donor favoured and disfavoured regions while violet and green cubes represent hydrophobic favoured and disfavoured regions respectively.

The atom based 3D QSAR model while predicting the biological activity takes into the account steric clashes apart from pharmacophore features where as pharmacophore based 3D QSAR predicts the biological activity depending on pharmacophore sites and their areas. From Figure 4a it can be seen that the NH of the indole ring, amino group of pyrimidine ring, NH attached to pyrazine ring and dimethyl amine groups were superposed onto the H-bond donor favoured pink contours.One of the nitrogen‘s of pyrazine ring is projecting into the blue H-bond acceptor favoured contours (Figure 4a). It matched with the H-bond acceptor feature A2 in the hypothesis. The NH of indole ring superposed onto the H-bond donor feature (yellow contour) is depicted in Figure 4b. It explicitly matched with the pharmacophoric feature D3. The dimethyl amino group was onto the H-bond donor favoured yellow contour (Figure 4b). The nitrogen’s of pyrazine and pyrimidine rings were placed towards hydrogen bond disfavoured orange contours (Figure 4b). In Figure 4c it can be observed that the hydrophilic favoured amine group and nitrogen's of the pyrimidine ring, one of the nitrogen's of pyrazine and the dimethyl amine were superposed onto the green hydrophilic favoured contours (Figure 4c).The presence of extra H-bond acceptor, donor and hydrophilic features is advantageous for the biological activity.

Pharmacophore Model Based Virtual Screening

Asinex and Otava lead library databases prepared earlier using LigPrep was used to screen in order to identify potential pim-3 inhibitors using ADRRR common pharmacophore hypothesis as the template. In this process of searching the conformers generated from the database were screened to match the CPH based on the site distance. Five out of five pharmacophore sites without partial matches were matched with the hypothesis in the present study. The search process resulted in the 1507 molecules out of total 186473 molecules from both Asinex and Otava lead library databases. The obtained hits will definitely act as promising pim-3 inhibitors since the model was developed from the active set of compounds with high inhibitory activity against pim-3. Therefore screened out ligands were further subjected to virtual screening process.

Validation Of 3d Model

The modelled protein was validated using ramachandran plot (PROCHECK), ERRAT, Verify 3D and ProSA (Protein Structure Analysis Server). Initially the detailed stereo chemical quality of each amino acid residue was evaluated by ramachandran plot employing PROCHECK program. The statistics of the modelled protein is shown in Figure 5. The modelled protein has 295 amino residues out of which 240 (96%) residues were in the most favoured regions, 9 (3.6%) residues were in additionally allowed regions and one (0.4%) residue was in generously allowed regions. Interestingly none of the amino acid residues were in disallowed regions excluding proline and glycine. The results from PROCHECK were promising hence the generated model is stereo chemically sterling. The information pertaining to non-bonded interactions between unlike atoms can be known by ERRAT. It is "overall quality factor", higher the score higher the quality. The acceptable range is >50 for a high quality model [56]. The overall quality factor i.e.

ERRAT score for generated model was 73.801 (Figure 6) indicating dependability and good stability of the protein [57]. The compatibility of an atomic model (3D) with its sequence (1D) can be analyzed by Verify 3D. The assigned 3D-1D score should never be below zero and should be above 0.2. In present study, the value was above 0.2 most part (Figure 7) indicating good compatibility of the model with its own sequence of amino acids. ProSA was used to compute the interaction energy per residue. In present case, the interaction energy of each amino acid residue was determined with respect to remaining protein in order to judge the energy criteria. The overall quality of the model can be assessed with ProSA Z-score. The quality of the protein using the Z-score is actually estimated by comparing the experimentally determined proteins with similar number of amino acid residues that were deposited in the protein databank by X-ray crystallographic method (light blue) and NMR spectroscopy (dark blue) (Figure 8a). The Z-score of the modelled protein was -7.1 (Figure 8b). This negative value indicates that the overall quality of the protein is good. All the above investigations suggest that a high quality model of pim-3 (Figure 9) was obtained which can be further used for docking and MD simulations.

Virtual Screening Using Glide

The 1507 hits filtered out from the Asinex and Otava lead library databases were docked into the active site of pim-3 in two stages. Initially all the hits restituted from the pharmacophore based screening were taken for docking using SP (standard precision) protocol. Subsequently, the selected top scoring 297 (20%) molecules obtained from SP docking were subjected to more rigorous XP (extra precision) docking. Finally binding energies were calculated and the top 6 (2%) molecules having binding energy values greater than the best active compound in the dataset were retrieved.

Binding Free Energy Calculations

The binding free energies of top 6 hits were computed and tabulated in the Table 3. The binding energies of the hits ranged from -94.698 to -96.128 Kcal/mol. The binding energy value of the best active compound (Table 3) was -94.419 Kcal/mol. All the screened ligands exhibited good binding energies greater than the best active compound. Therefore it is clear that these molecules can definitely have greater probability of becoming potent inhibitors against pim-3.

Table 3
Binding free energies of top hits retrieved from Asinex and Otava lead library databases

S. No.	Compound	Binding Energy (Kcal/mol)
1.	39 (Best active)	-94.419
2.	N1	-96.128
3.	N2	-96.075
4.	N3	-95.659
5.	N4	-95.270
6.	N5	-94.836
7.	N6	-94.698

Interaction Studies Of Screened Hits

The interaction patterns of the screened hits were analyzed from Ligand Interaction Diagram (LID) available in the Schrodinger suite. The interactions are shown in Figures 10 and 11. The purple lines indicate hydrogen bond interactions, green lines indicate π-π stacking interactions, red lines indicate π-cationic interactions and blue-pink line indicates salt bridges. Initially, the pim-3 best active complex was examined with the help of LID. The result is illustrated in Figure 10. The best active compound formed three hydrogen bond interactions with Glu 124, Asp 131 and Glu 174 and formed a salt bridge with Asp 189. The results of the screened hits are illustrated in Figure 11 and Supplementary Figure S1. The screened hits formed hydrogen bond interactions with Phe 51, Glu 124, Arg 125, Pro 126, Asp 131, Asp 134, Glu 174, Asp 189 and Phe 190, salt bridges with Asp 131and Asp189 and showed π-π stacking and π-cationic interactions with Phe 51.

Molecular Dynamics Simulations

The molecular interactions which are actually accountable for the stability are explored with the help of molecular dynamics simulation. To investigate the stability and molecular interactions of the screened hit (N1) obtained from Asinex and Otava lead library databases, MD simulations were performed for 10 ns. The RMSD of screened hit (N1) complexed with pim-3 is shown in the Figure 12. The RMSD initially reached to 2.64Å at 0.74 ns from 1.57Å around 50 ps. The RMSD after fluctuating aroused to 3.54 Å around 4.76 ns and retained between 2.68 and 3.99 Å throughout the simulation up to 10 ns. The

averaged RMSD of the complex was 3.11Å indicating that the screened hit N1 formed a stable complex with pim-3.

Protein-ligand interactionsis one of the major factors that is analyzed during the course of simulation. They are useful in understanding the dynamic changes and binding modes during MD simulations. There are four substantial protein-ligand contacts or interactions in MD simulations namely hydrogen bonding, ionic, hydrophobic and water bridges. The binding site of pim-3 consisted the following amino acid residuesPhe 51, Glu 124, Arg 125, Pro 126, Asp 131, Asp 134, Glu 174, Asp 189 and Phe 190.

The screened hit N1 showed hydrogen bond interaction with Glu 124 (96.90%), hydrophobic interactions with Val 54 (19.38%), Ala 67 (45.25%), Leu 123 (58.44%), Leu 177 (34.06%) and Ile 188 (49.45%) and formed water mediated hydrogen bonds with Leu 46 (18.68%), Pro 126 (10.78%), Lys 172 (10.18%), Glu 174 (35%) and Asp 189 (6.69%) (Figures 13 and 14). It also formed π-π stacking and π-cationic interactions with Phe 51 for 71% and 54% of simulation time respectively (Figure 13 and 14). Surprisingly ionic interactions were lost and not observed in the protein complex N1. Therefore it can be noted that the screened hit N1 has good interactions with pim-3.

Conclusions

The aim of the present study is used to identify new potent and promising hits against pim-3 by employing diverse computational methods. To achieve the purpose pharmacophore based virtual screening, homology modelling, molecular docking, binding free energy analysis and molecular dynamics simulation techniques were used. Initially a pharmacophore model (ADRRR) was derived using reported pim-3 inhibitors which were used to screen the subsets of molecules from Asinex and Otava lead library databases. Later molecular docking and binding free energies were performed on the retrieved hits which ultimately yielded 6 hits with binding free energies greater than that of best active molecule. Actually the crystal structure of pim-3 was not available hence homology modelling was employed to model the protein. Finally MD simulations were carried out on the top hit with highest binding energy which showed stable binding with that of the target pim-3. All in all, the study suggests that integrated 3D QSAR, homology modelling, molecular docking, binding free energy analysis and MD simulation techniques can be helpful in identifying new pim-3 inhibitors. The inference drawn in the current study can provide some insights to the research community to discover new potent inhibitors against pim-3 with greater biological activity.

Declarations

Supplementary Information

Supplementary information consists of Inter-pharmacophoric site distances and angle measurements of the model ADRRR (Tab S1 and Tab S2) and Ligand interaction diagrams of screened hits (N2 to N6) retrieved from Asinex and Otava lead library databases (Figure S1).

Acknowledgements

We greatly acknowledge Tripos Inc., USA and Schrödinger LLC, New York for providing the software. The author Peddi Sudhir Reddy would like to acknowledge financial support from UGC for a research fellowship.

Author Contribution

Sudhir Reddy Peddi: Conceptualization, Methodology, Investigation, Software, Visualization, Data curation, Validation, Resources, Writing-original draft. **Ramalingam Kundenapally:** Investigation, Visualization, Data curation, Validation, Formal analysis. **Sreekanth Sivan:** Writing-review & editing, Validation, Visualization, Formal analysis. **Gururaj Somadi:** Investigation, Visualization, Formal analysis. **Vijjulatha Manga:** Software, Supervision, Funding acquisition, Project administration.

Funding

This work was supported by Council of Scientific and Industrial Research [02(0379)/19/EMR-II].

Availability of Data and material

Not Applicable.

Code availability

Not Applicable.

Declarations

No potential conflict of interest was reported by the authors.

References

1. Feldman JD, Vician L, Crispino M, Tocco G, Marcheselli VL, Bazan NG, Baudry M, Herschman HR (1998) KID-1, a protein kinase induced by depolarization in brain. J Biol Chem 273(26):16535-43
2. Nawijn MC, Alendar A, Berns A (2011) For better or for worse: the role of Pim oncogenes in tumorigenesis. Nat Rev Cancer 11(1):23-34
3. Fujii C, Nakamoto Y, Lu P, Tsuneyama K, Popivanova BK, Kaneko S, Mukaida N (2005) Aberrant expression of serine/threonine kinase Pim-3 in hepatocellular carcinoma development and its role in the proliferation of human hepatoma cell lines. Int J Cancer 114(2):209-18
4. Brault L, Gasser C, Bracher F, Huber K, Knapp S, Schwaller J (2010) PIM serine/threonine kinases in pathogenesis and therapy of hematological malignancies and solid cancers. Haematologica 95:1004–1015

5. Li YY, Popivanova BK, Nagai Y, Ishikura H, Fujii C, Mukaida N (2006) Pim-3, a proto-oncogene with serine/threonine kinase activity, is aberrantly expressed in human pancreatic cancer and phosphorylates bad to block bad-mediated apoptosis in human pancreatic cancer cell lines. Cancer Res 66(13):6741-7
6. Popivanova BK, Li YY, Zheng H, Omura K, Fujii C, Tsuneyama K, Mukaida N (2007) Proto-oncogene, Pim-3 with serine/threonine kinase activity, is aberrantly expressed in human colon cancer cells and can prevent Bad-mediated apoptosis. Cancer Sci 98(3):321-8
7. Liu J, Qu X, Shao L, Hu Y, Yu X, Lan P, Guo Q, Han Q, Zhang J, Zhang C (2018) Pim-3 enhances melanoma cell migration and invasion by promoting STAT3 phosphorylation. Cancer Biol Ther 19:160–168
8. Mukaida N, Wang YY, Li YY (2011) Roles of Pim-3, a novel survival kinase, in tumorigenesis. Cancer Sci 102(8):1437-42
9. Zheng HC, Tsuneyama K, Takahashi H, Miwa S, Sugiyama T, Popivanova BK, Fujii C, Nomoto K, Mukaida N, Takano Y (2008) Aberrant Pim-3 expression is involved in gastric adenoma-adenocarcinoma sequence and cancer progression. J Cancer Res Clin Oncol 134(4):481-8
10. Deneen B, Welford SM, Ho T, Hernandez F, Kurland I, Denny CT (2003) PIM3 proto-oncogene kinase is a common transcriptional target of divergent EWS/ETS oncoproteins. Mol Cell Biol 23(11):3897-908
11. Li YY, Wu Y, Tsuneyama K, Baba T, Mukaida N (2009) Essential contribution of Ets-1 to constitutive Pim-3 expression in human pancreatic cancer cells. Cancer Sci 100(3):396-404
12. Chang M, Kanwar N, Feng E, Siu A, Liu X, Ma D, Jongstra J (2010) PIM kinase inhibitors downregulate STAT3(Tyr705) phosphorylation. Mol Cancer Ther 9(9):2478-87
13. Preethi B, Shanthi V, Ramanathan K (2015) Investigation of nalidixic acid resistance mechanism in salmonella enterica using molecular simulation techniques. Appl Biochem Biotechnol 177(2):528–540
14. Karthick V, Shanthi V, Rajasekaran R, Ramanathan K (2012) Exploring the cause of oseltamivir resistance against mutant H274Y neuraminidase by molecular simulation approach. Appl Biochem Biotechnol 167(2):237–249
15. Sliwoski G, Kothiwale S, Meiler J, Lowe EW (2014) Computational methods in drug discovery. Pharmacol Rev 66(1):334–395
16. James N, Ramanathan K (2018) Discovery of potent ALK inhibitors using pharmacophore-Informatics strategy. Cell Biochem Biophys 76(1-2):111–124
17. Dhanachandra Singh KH, Karthikeyan M, Kirubakaran P, Nagamani S (2011) Pharmacophore filtering and 3D-QSAR in the discovery of new JAK2 inhibitors. J Mol Graph Model 30:186–197
18. Dash RC, Bhosale SH, Shelke SM, Suryawanshi MR, Kanhed AM, Mahadik KR (2012) Scaffold hopping for identification of novel D(2) antagonist based on 3D pharmacophore modelling of illoperidone analogs. Mol Divers 16(2):367–375
19. Sudha A, Srinivasan P, Rameshthangam P (2015) Exploration of potential EGFR inhibitors: a combination of pharmacophore-based virtual screening, atom-based 3D-QSAR and molecular

docking analysis. J Recept Signal Transduct Res 35(2):137–148

20. Gogoi D, Baruah VJ, Chaliha AK, Kakoti BB, Sarma D, Buragohain AK (2016) 3D pharmacophore-based virtual screening, docking and density functional theory approach towards the discovery of novel human epidermal growth factor receptor-2 (HER2) inhibitors. J Theor Biol 411:68–80
21. More KN, Jang HW, Hong VS, Lee J (2014) Pim kinase inhibitory and antiproliferative activity of a novel series of meridianin C derivatives. Bioorg Med Chem Lett 24(11):2424-8
22. More KN, Hong VS, Lee A, Park J, Kim S, Lee J (2018) Discovery and evaluation of 3,5-disubstituted indole derivatives as Pim kinase inhibitors. Bioorg Med Chem Lett 28(14):2513-2517
23. Lee J, More KN, Yang S, Hong VS (2014) 3,5-Bis(aminopyrimidinyl) indole Derivatives: Synthesis and Evaluation of Pim Kinase Inhibitory Activities. Bull Korean Chem Soc 35(7):2123-2129
24. Khan MF, Verma G, Akhtar W, Shaquiquzzaman M, Akhter M, Rizvi MA, Alam MM (2019) Pharmacophore modeling, 3D-QSAR, docking study and ADME prediction of acyl 1, 3, 4thiadiazole amides and sulfonamides as antitubulin agents. Arab J Chem 12(8):5000-5018
25. Bhadoriya KS, Sharma MC, Jain SV (2015) 2, 4-Dihydropyrano [2, 3-c] pyrazole: Discovery of new lead as through pharmacophore modelling, atom-based 3D-QSAR, virtual screening and docking strategies for improved anti-HIV-1 chemotherapy. J Taibah Univ Sci 9(4):521–530
26. Sadowski J, Rudolph C, Gasteiger J (1992) The generation of 3D models of host-guest complexes. Analytica Chimica Acta 265(2):233–241
27. Dixon SL, Smondyrev AM, Knoll EH, Rao SN, Shaw DE, Friesner RA (2006) PHASE: a new engine for pharmacophore perception, 3D QSAR model development, and 3D database screening: 1. Methodology and preliminary results. J Comput Aided Mol Des 20(10-11):647–671
28. Kirubakaran P, Muthusamy K, Singh KH, Nagamani S (2012) Ligand-based pharmacophore modeling; atom-based 3D-QSAR analysis and molecular docking studies of phosphoinositide-dependent kinase-1 inhibitors. Indian J Pharm Sci 74(2):141-151
29. Silakari O, Chand S, Bahia MS (2012) Structural basis of amino pyrimidine derivatives for inhibitory activity of PKC-θ: 3D-QSAR and molecular docking studies. Mol Inform 31(9):659–668
30. Golbraikh A, Shen M, Xiao Z, Xiao YD, Lee KH, Tropsha A (2003) Rational selection of training and test sets for the development of validated QSAR models. J Comput Aided Mol Des 17(2-4):241–253
31. Pan Y, Wang Y, Bryant SH (2013) Pharmacophore and 3D-QSAR characterization of 6 arylquinazolin-4-amines as Cdc2-like kinase 4 (Clk4) and dual specificity tyrosine-phosphorylation-regulated kinase 1A (Dyrk1A) inhibitors. J Chem Inf Model 53(4):938–947
32. Magrane M, UniProt consortium (2011) UniProt Knowledgebase: a hub of integrated protein data. Database (Oxford) 2011:bar009
33. Johnson M, Zaretskaya I, Raytselis Y, Merezhuk Y, McGinnis S, Madden TL (2008) NCBI BLAST: a better web interface. Nucleic Acids Res 36(Web Server issue):W5–W9
34. Chenna R, Sugawara H, Koike T, Lopez R, Gibson TJ, Higgins DG, Thompson JD (2003) Multiple sequence alignment with the Clustal series of programs. Nucleic Acids Res 31(13):3497–500

35. Sali A, Potterton L, Yuan F, Van Vlijmen H, Karplus M (1995) Evaluation of comparative protein modelling by MODELLER. Proteins 23(3):318–326
36. Laskowski RA, Mac Arthur MW, Moss DS, Thornton JM (1993) PROCHECK: a program to check the stereochemical quality of protein structures. J Appl Cryst 26:283–91
37. Eisenberg D, Lüthy R, Bowie JU (1997) VERIFY3D: assessment of protein models with three-dimensional profiles. Methods Enzymol 277:396–404
38. Wiederstein M, Sippl MJ (2007) ProSA-web: interactive web service for the recognition of errors in three-dimensional structures of proteins. Nucleic Acids Res 35(Web Server issue):W407–W410
39. Sali A, Kuriyan J (1999) Challenges at the frontiers of structural biology. Trends Cell Biol 9(12):M20–M24
40. Schrödinger LLC, 2010 Glide, Version 5.6. New York, NY
41. Halgren TA, Murphy RB, Friesner RA, Beard HS, Frye LL, Pollard WT, Banks JL (2004) Glide: a new approach for rapid, accurate docking and scoring. 2. Enrichment factors in database screening. J Med Chem 47(7):1750–1759
42. Elancheran R, Saravanan K, Choudhury B, Divakar S, Kabilan S, Ramanathan M, Das B, Devi R, Kotoky J (2016) Design and development of oxobenzimidazoles as novel androgen receptor antagonists. Med Chem Res 25(4):539–552
43. Friesner RA, Banks JL, Murphy RB, Halgren TA, Klicic JJ, Mainz DT, Repasky MP, Knoll EH, Shelley M, Perry JK, Shaw DE, Francis P, Shenkin PS (2004) Glide: a new approach for rapid, accurate docking and scoring. 1. Method and assessment of docking accuracy. J Med Chem 47(7):1739-49
44. Lyne PD, Lamb ML, Saeh JC (2006) Accurate prediction of the relative potencies of members of a series of kinase inhibitors using molecular docking and MM-GBSA scoring. J Med Chem 49(16):4805–4808
45. Shaw DE, 2014. Desmond, Version 3.8. New York, NY
46. Berendsen HJC, Grigera JR, Straatsma TP (1987) The missing term in effective pair potentials. J Phys Chem 91(24):6269–6271
47. Kaminski GA, Friesner RA, Tirado-Rives J, Jorgensen WL (2001) Evaluation and reparametrization of the OPLS-AA force field for proteins via comparison with accurate quantum chemical calculations on peptides. J Phys Chem B 105(28):6474–6487
48. Strahan GD, Keniry MA, Shafer RH (1998) NMR structure refinement and dynamics of the K+-$[d(G3T4G3)]_2$ quadruplex via particle mesh Ewald molecular dynamics simulations. Biophys J, 75(2):968–981
49. Andersen HC (1983) Rattle: A “velocity” version of the shake algorithm for molecular dynamics calculations. J Comput Physics 52(1):24–34
50. Teli MK, Rajanikant GK (2012) Pharmacophore generation and atom-based 3D-QSAR of novel quinoline-3-carbonitrile derivatives as Tpl2 kinase inhibitors. J Enzyme Inhib Med Chem 27(4):558–570

51. Ugale VG, Patel HM, Surana SJ (2013) Molecular modeling studies of quinoline derivatives as VEGFR-2 tyrosine kinase inhibitors using pharmacophore based 3D QSAR and docking approach. Arab J Chem 10(2):S1980–S2003
52. Mahipal, Tanwar OP, Karthikeyan C, Moorthy NS, Trivedi P (2010) 3D QSAR of aminophenyl benzamide derivatives as histone deacetylase inhibitors. Med Chem 6(5):277–285
53. Chaudhari P, Bari S (2016) In silico exploration of c-KIT inhibitors by pharmaco-informatics methodology: pharmacophore modeling, 3D QSAR, docking studies, and virtual screening. Mol Divers 20(1):41–53
54. Kristam R, Parmar V, Viswanadhan VN (2013) 3D-QSAR analysis of TRPV1 inhibitors reveals a pharmacophore applicable to diverse scaffolds and clinical candidates. J Mol Graph Model 45:157–172
55. Morya VK, Dewaker V, Kim EK (2012) In silico study and validation of phosphotransacetylase (PTA) as a putative drug target for Staphylococcus aureus by homology-based modelling and virtual screening. Appl Biochem Biotechnol 168(7):1792–1805
56. Colovos C, Yeates TO (1993) Verification of protein structures: patterns of non-bonded atomic interactions. Protein Sci 2:1511–19
57. Mahgoub EO, Bolad A (2013) Correctness and accuracy of template-based modeled single chain fragment variable (scFv) protein anti-breast cancer cell line (MCF-7). Open J Genet 3:183–194

Figures

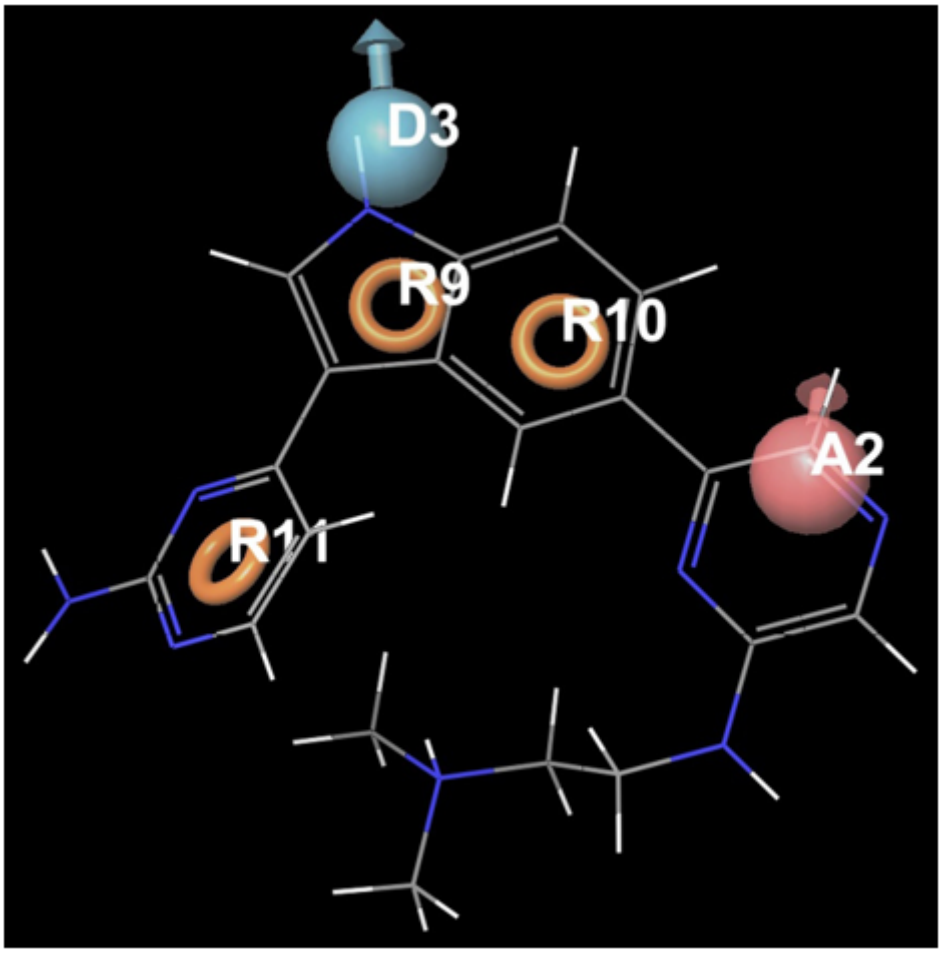

Figure 1

Description of five featured pharmacophore model ADRRR where pink and blue sphere with vectors symbolizes H-bond acceptor and donor features and three orange rings typifies aromatic ring features respectively

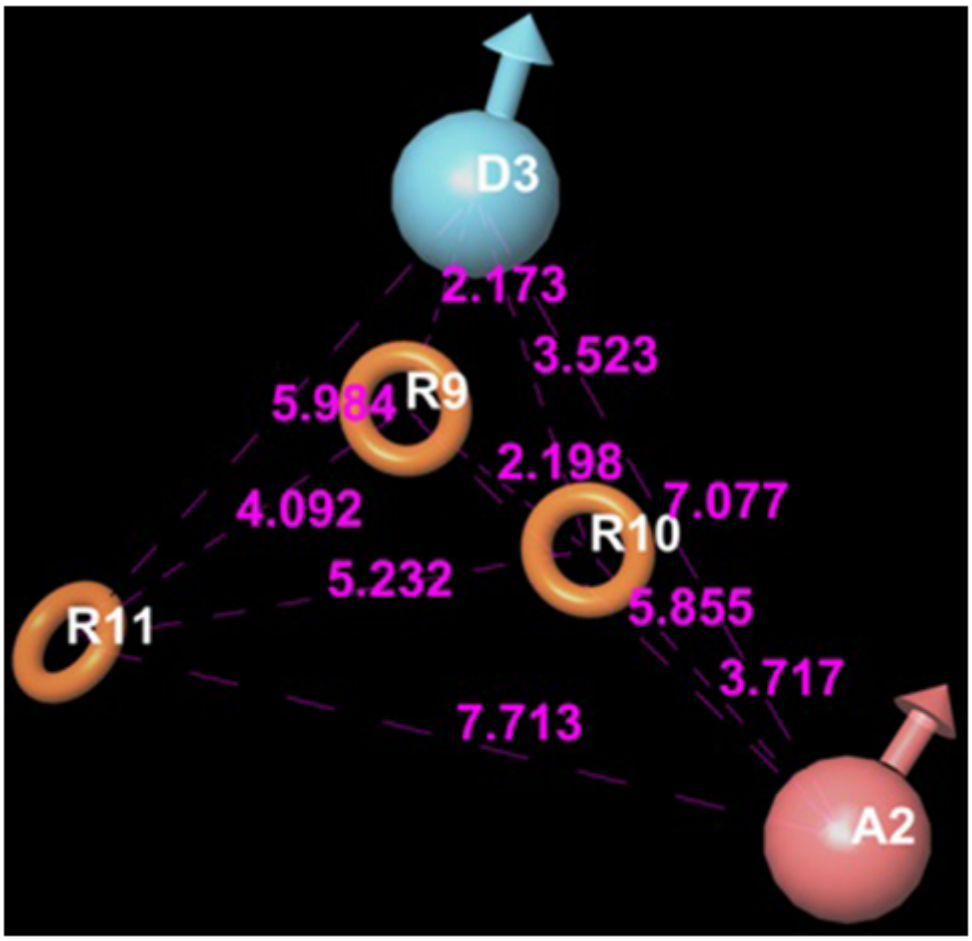

Figure 2

Inter-pharmacophore site distances of the model ADRRR

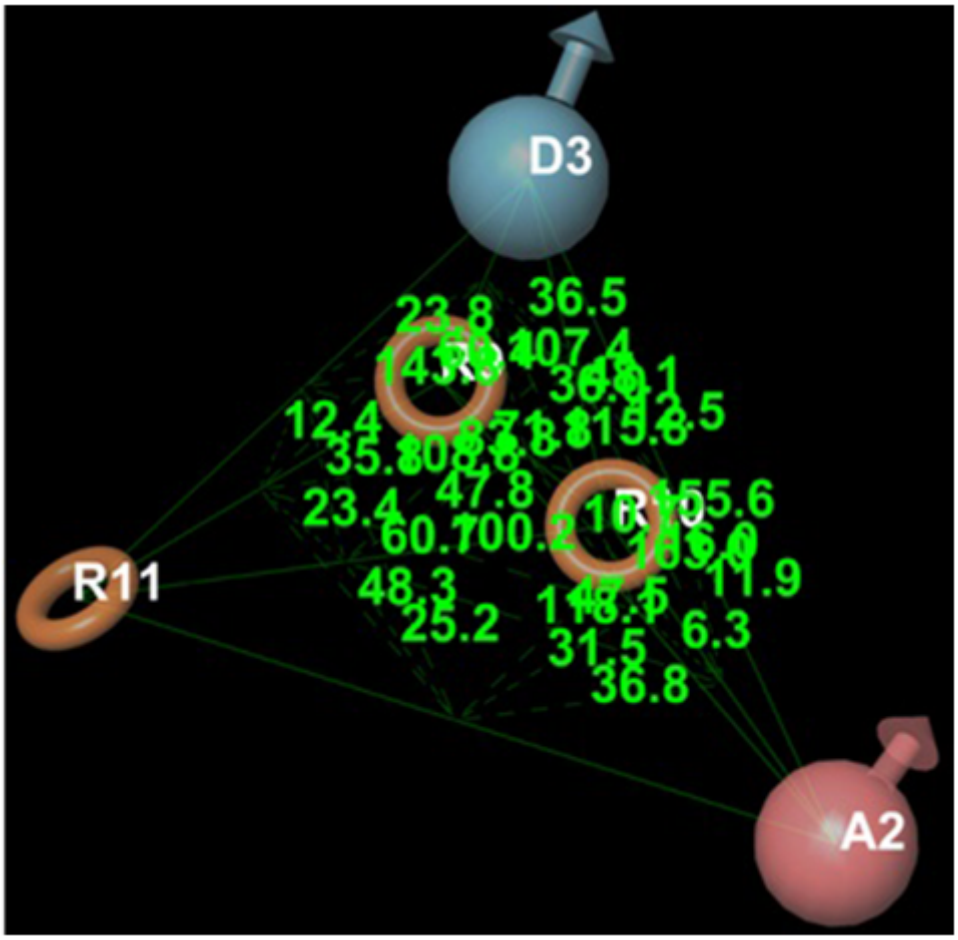

Figure 3

Inter-pharmacophore angle measurements of the model ADRRR

Figure 4

Visualization of 3D QSAR model in connection with compound 39 (best active compound) emphasizing the effect of (a) H-bond acceptor (b) H-bond donor and (c) hydrophobic features.

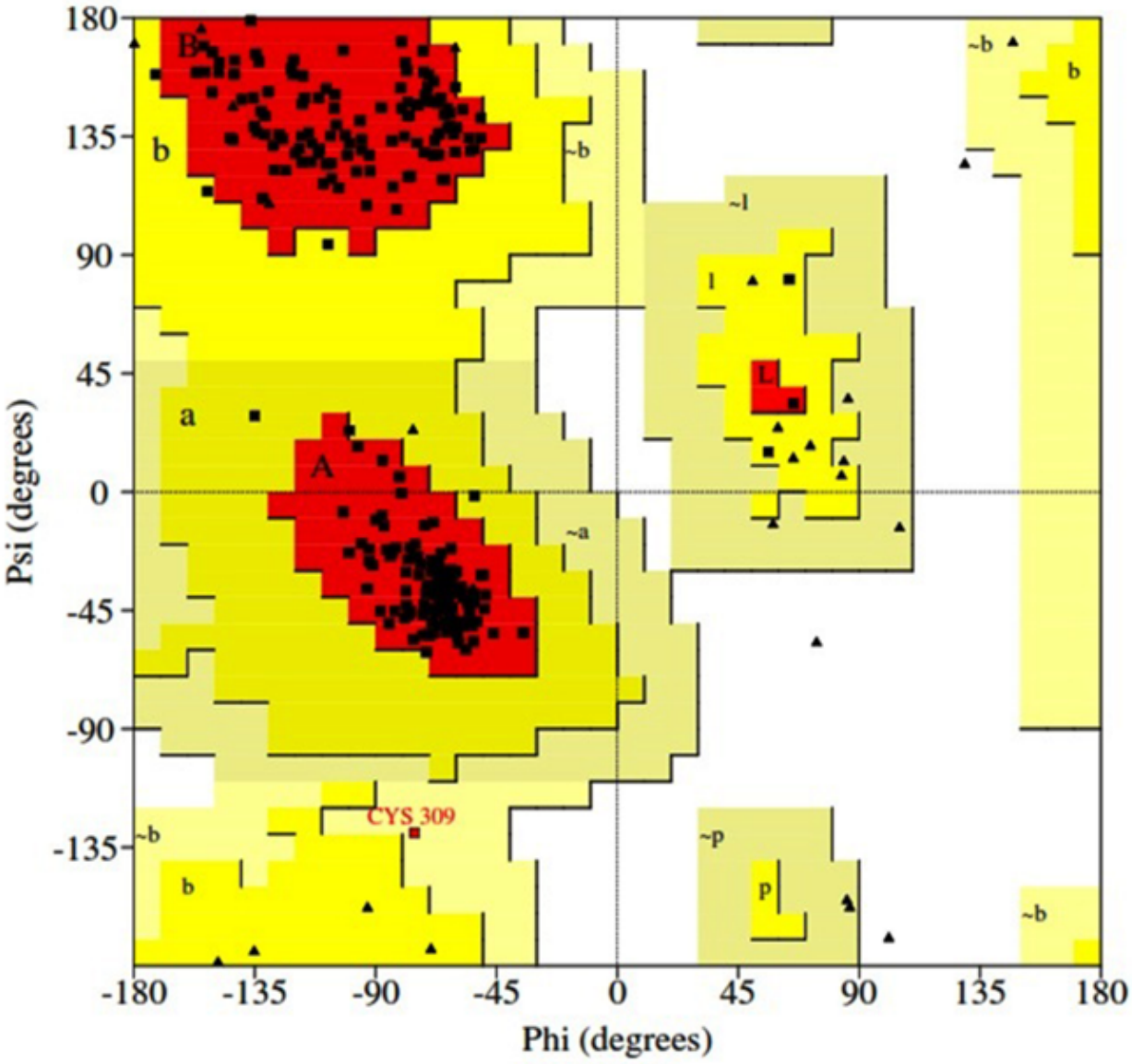

Figure 5

Ramachandran plot of the modelled pim-3 protein obtained from PROCHECK server

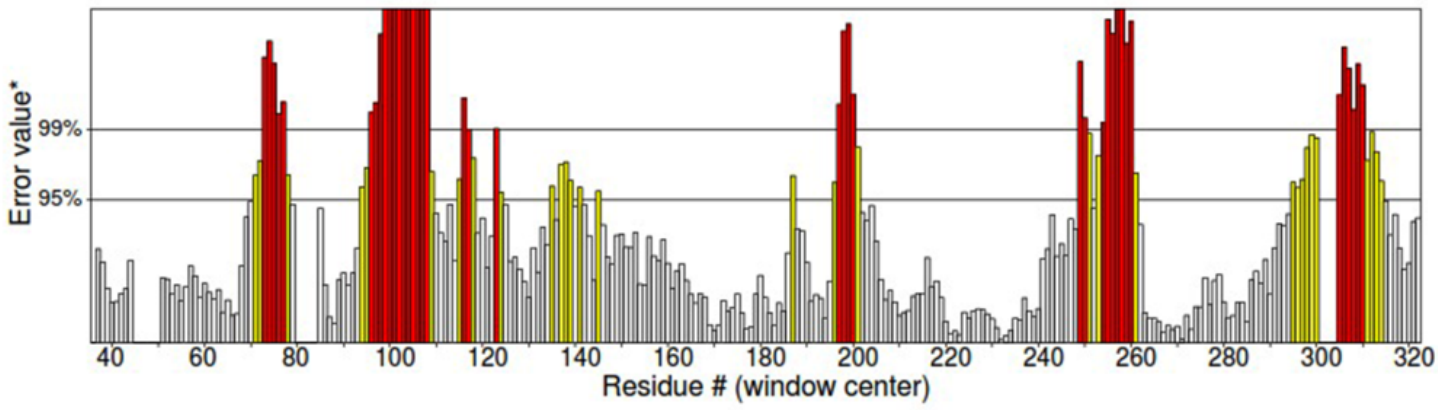

Figure 6

Overall quality factor (ERRAT) of pim-3 protein retrieved from SAVES server

Figure 7

Plot obtained from verify 3D depicting the compatibility of modelled pim-3 protein

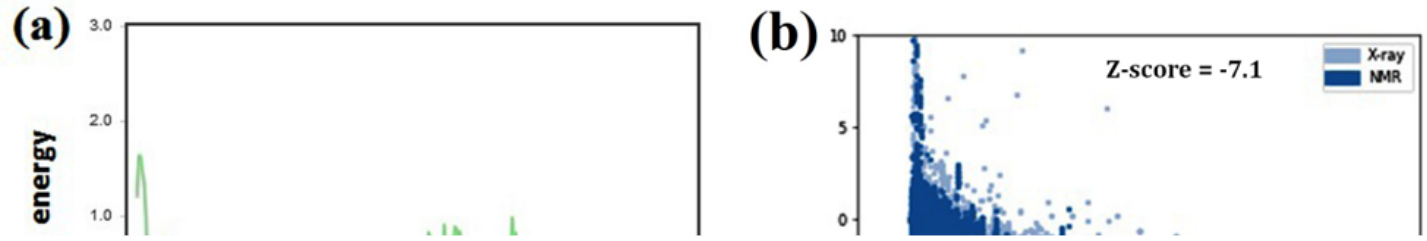

Figure 8

(a) ProSA energy profile of modelled pim-3 protein illustrating the local model quality. (b) Negative Z-score (-7.1) indicating overall good quality model of pim-3 protein compared to amino acids deposited in the protein data bank

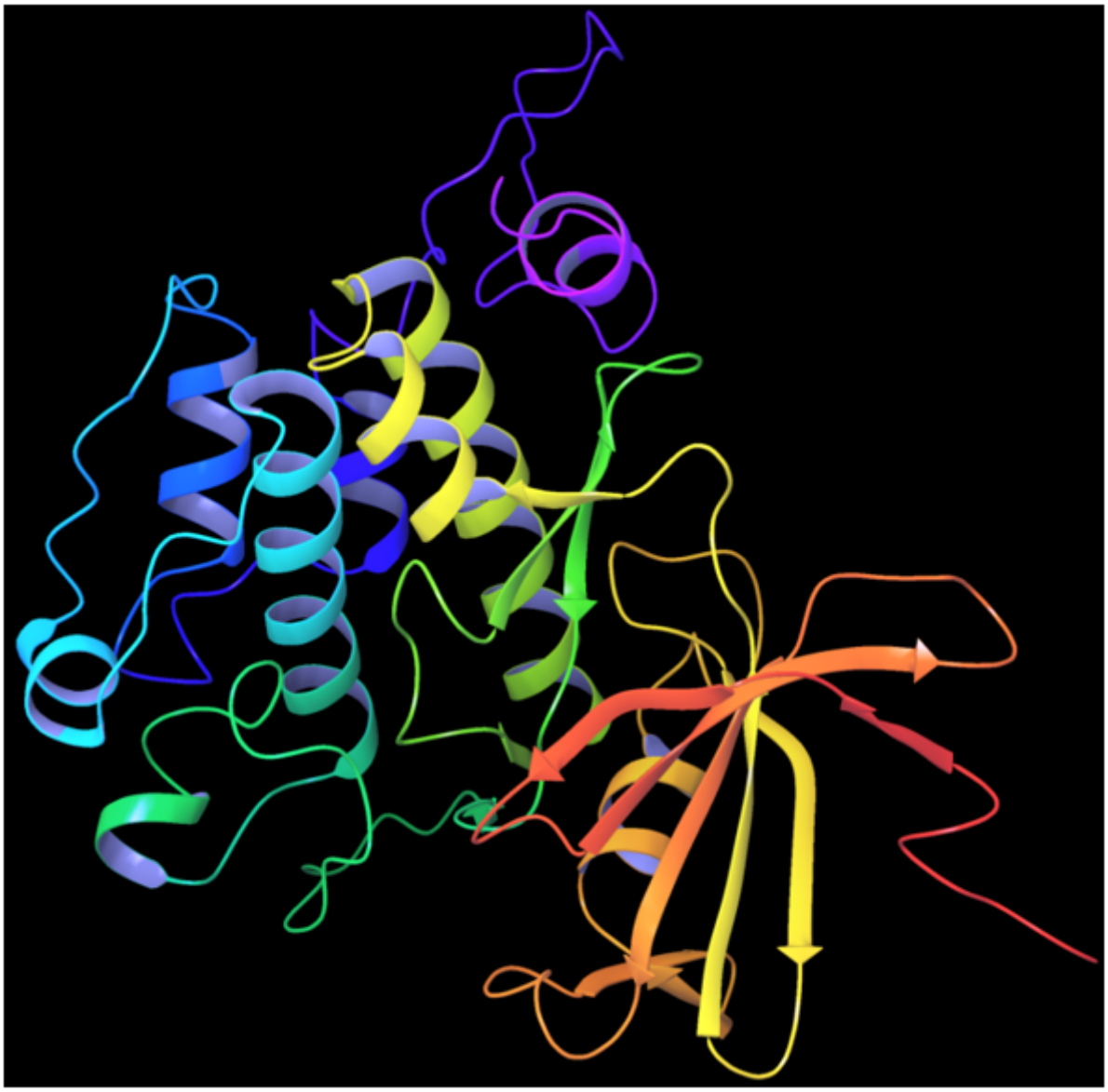

Figure 9

3D modelled structure of pim-3 protein

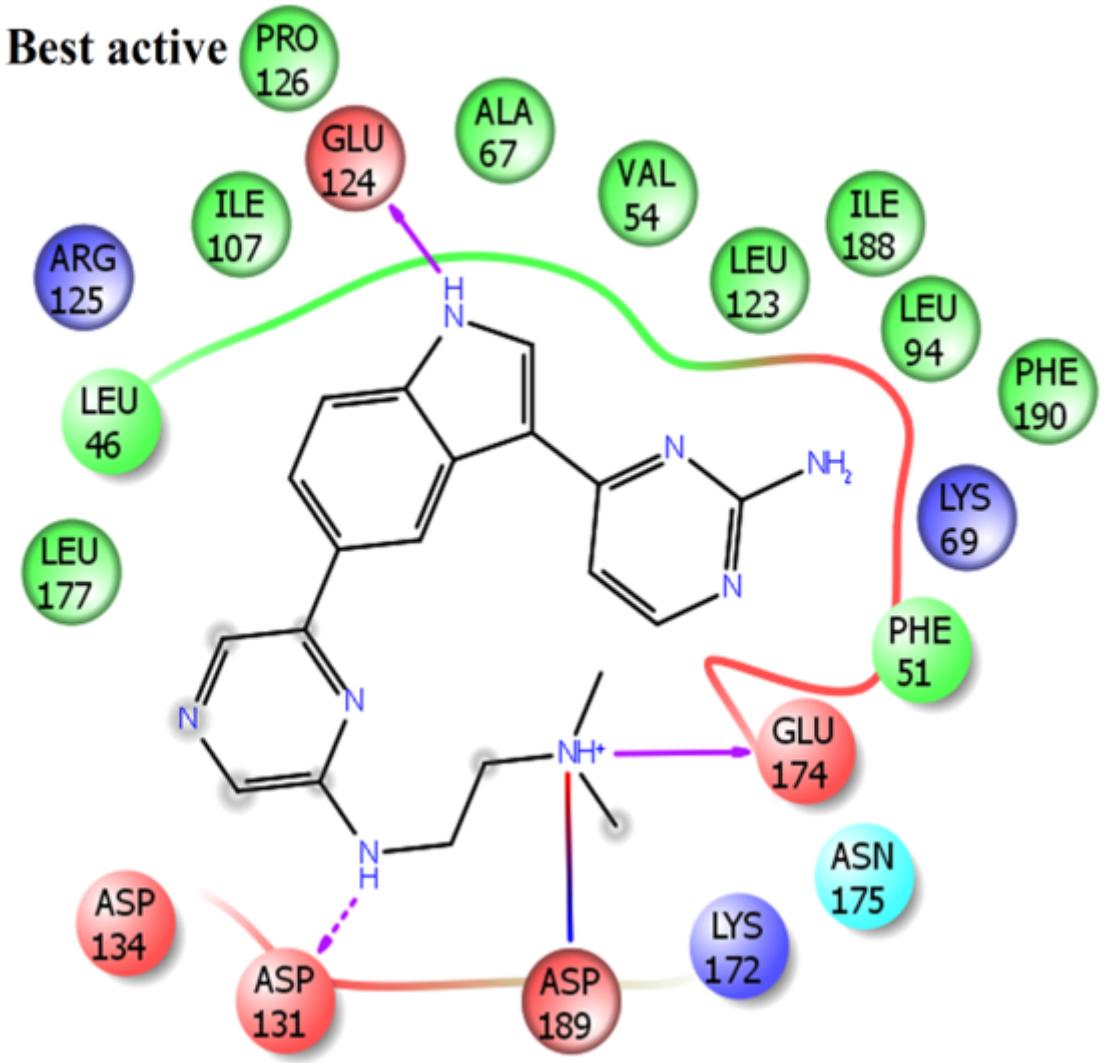

Figure 10

Ligand interaction diagram of best active compound (compound 39) with active site of pim-3

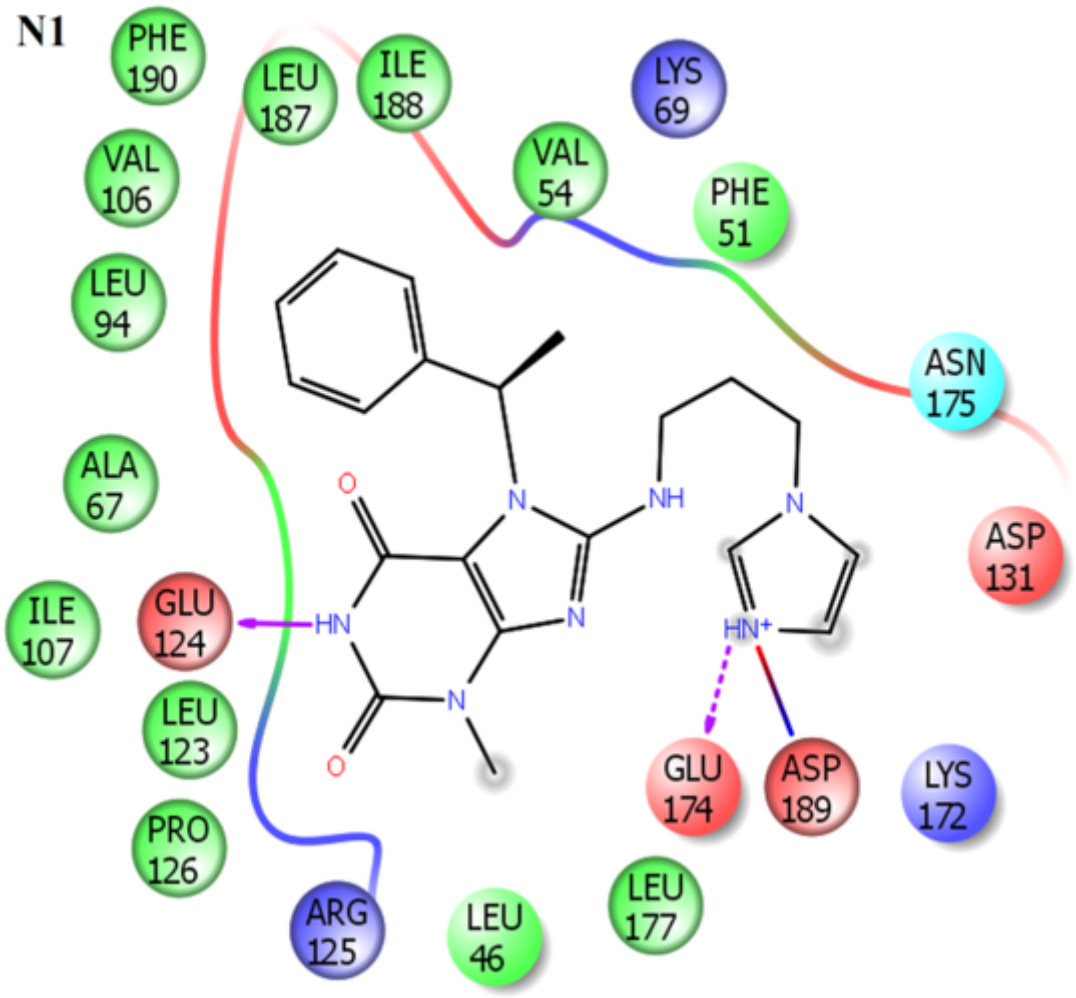

Figure 11

Ligand interaction diagram of molecule N1 obtained from Asinex and Otava lead library databases

Figure 12

RMSD (root mean square deviation) plot of screened hit (N1) complexed with pim-3 as a function of simulation time with respect to initial structure

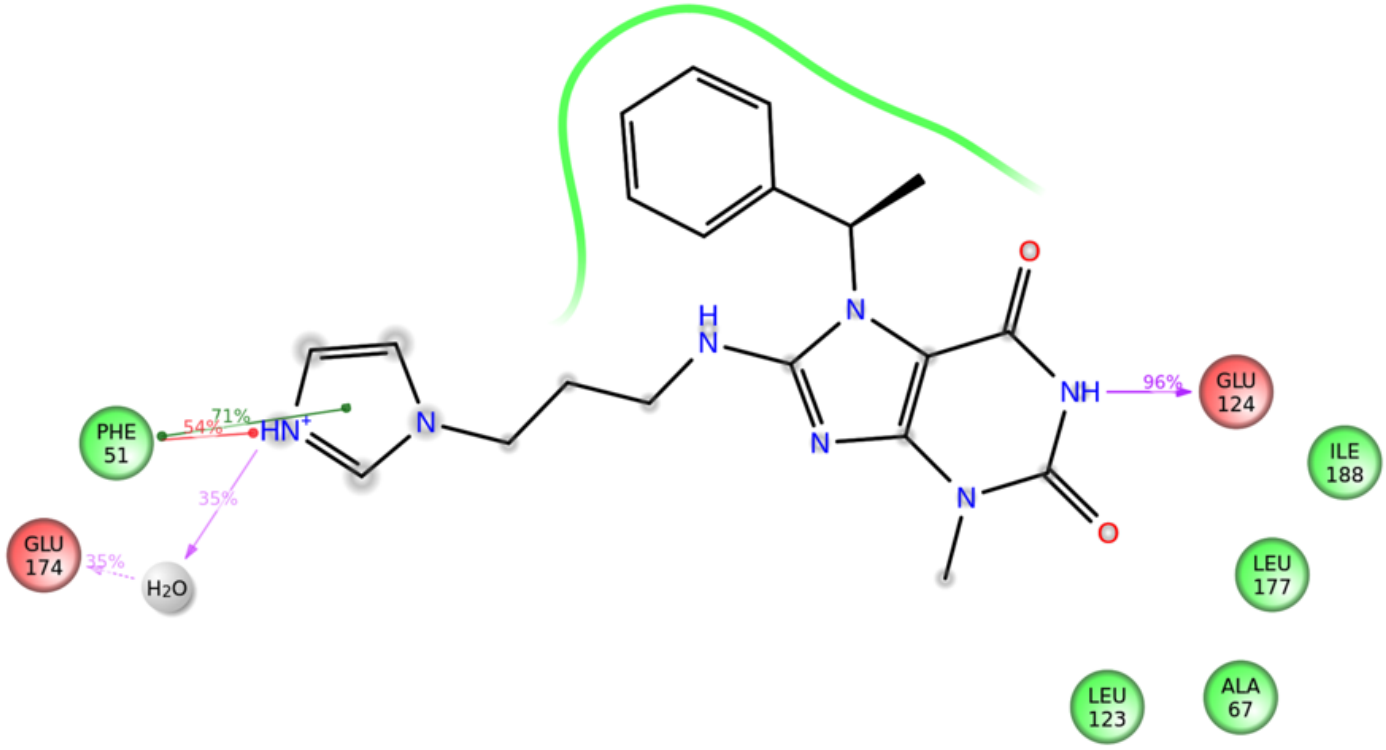

Figure 13

Average conformation of the binding pocket of pim-3 complexed with screened hit (N1) throughout the simulation of 10 ns

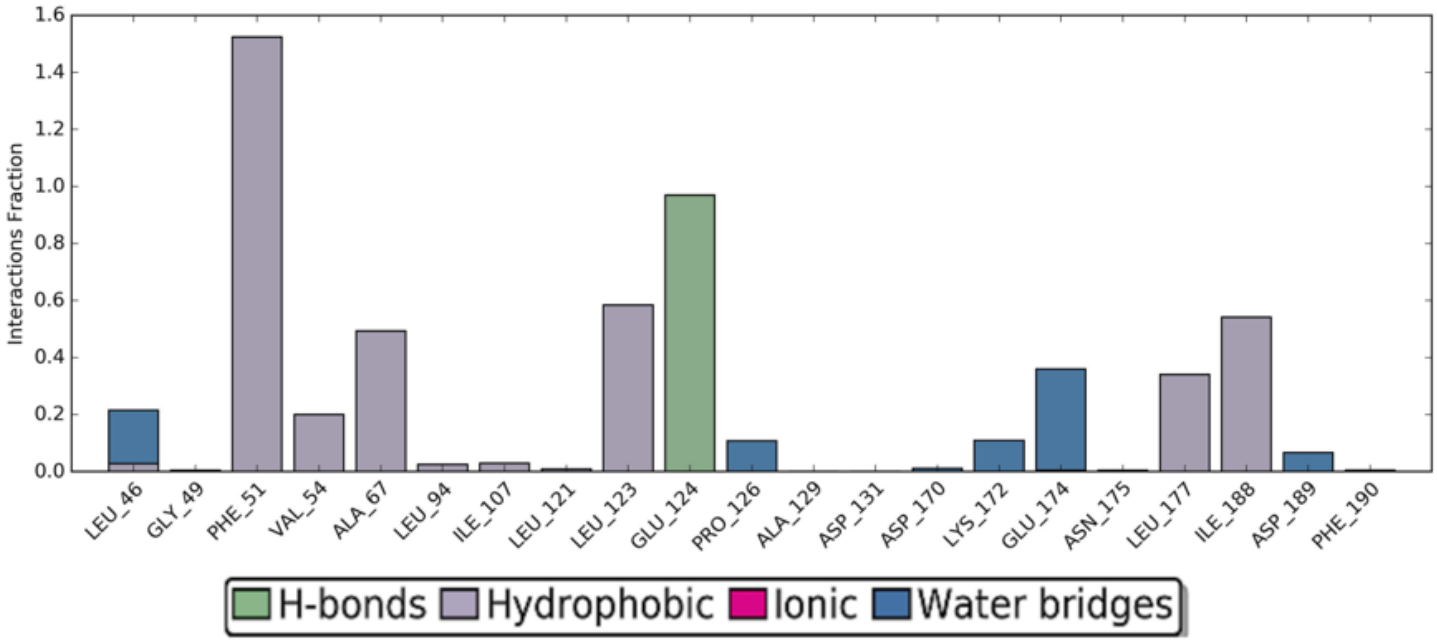

Figure 14

Protein-ligand interactions over trajectory with respect to screened hit (N1)

Supplementary Files

This is a list of supplementary files associated with this preprint. Click to download.

- Supplementary.docx